AD-A094 122 AIR FORCE GEOPHYSICS LAB HANSCOM AFB MA F/G 20/8
P78-2 SCATHA PRELIMINARY DATA ATLAS.(U)
AUG 80 E G MULLEN, H B GARRETT, D A HARDY
UNCLASSIFIED AFGL-TR-80-0241 NL

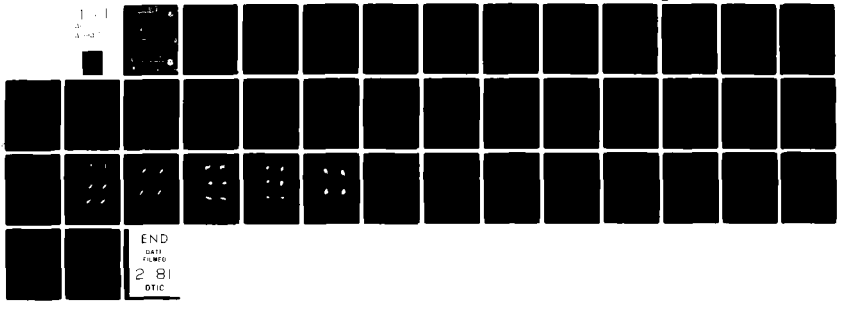

END
DATE FILMED
2 81
DTIC

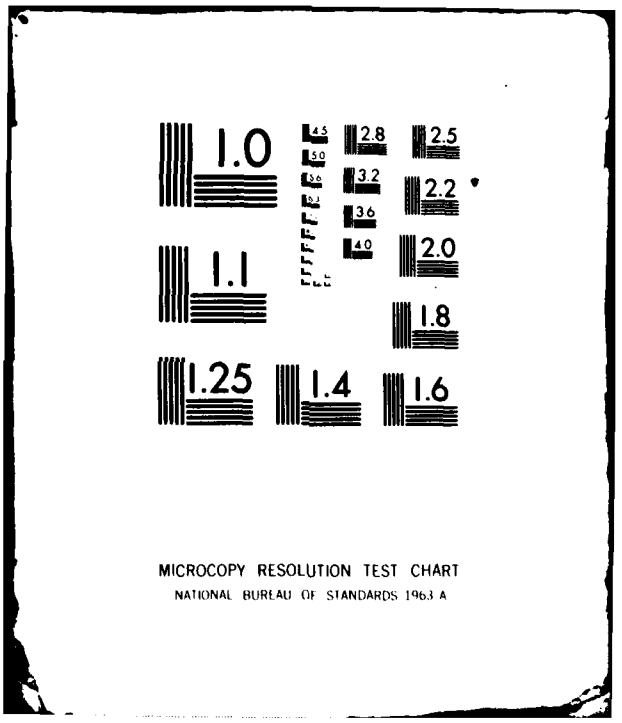
1.0
1.1
1.25
1.4
1.6
1.8
2.0
2.2
2.5
2.8
3.2
3.6
4.0
4.5
5.0
MICROCOPY RESOLUTION TEST CHART
NATIONAL BUREAU OF STANDARDS 1963 A

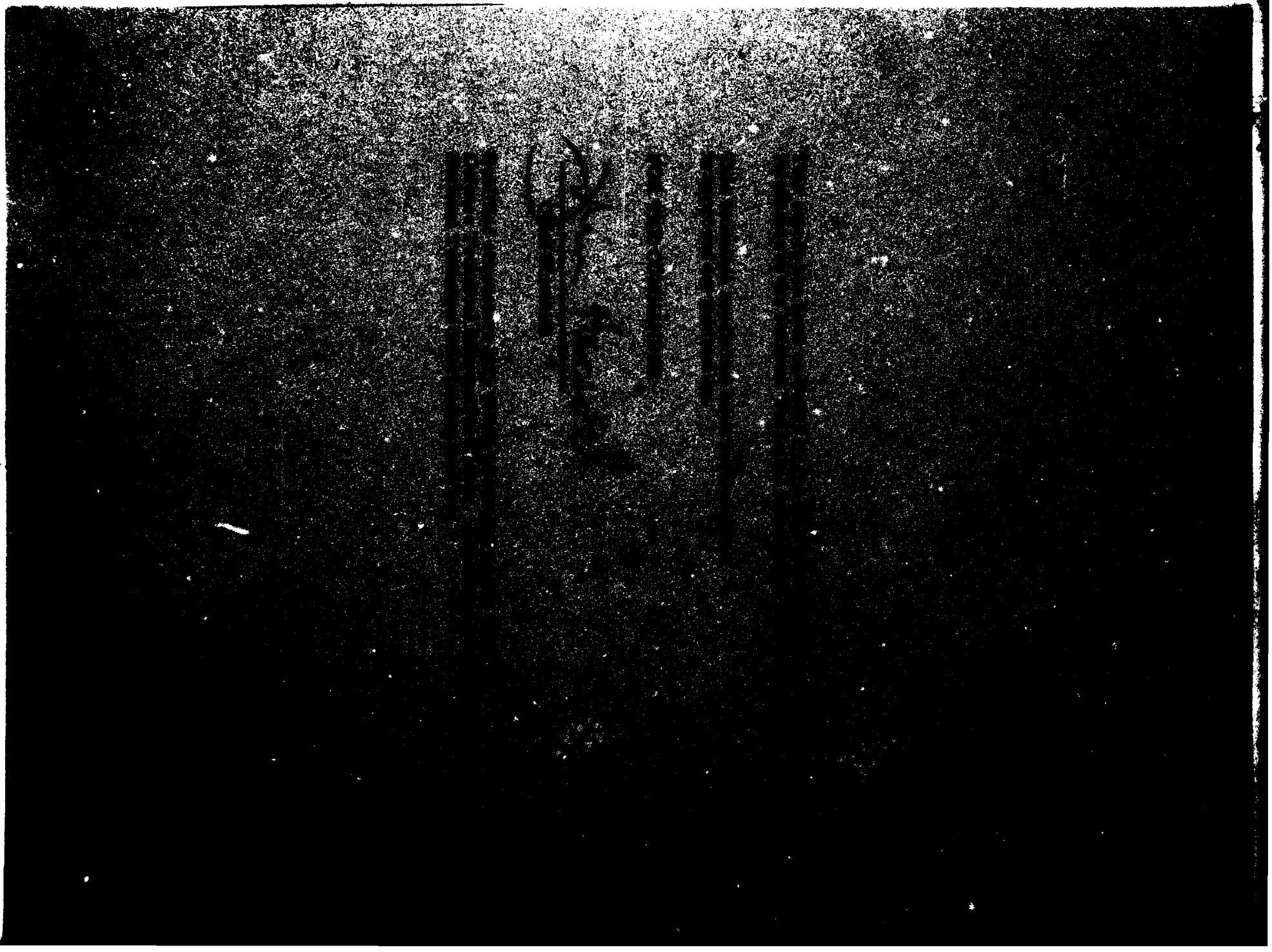

Unclassified

SECURITY CLASSIFICATION OF THIS PAGE (When Data Entered)

REPORT DOCUMENTATION PAGE	READ INSTRUCTIONS BEFORE COMPLETING FORM
1. REPORT NUMBER AFGL-TR-80-0241	2. GOVT ACCESSION NO. AD-A094122
3. RECIPIENT'S CATALOG NUMBER	
4. TITLE (and Subtitle) P78-2 SCATHA PRELIMINARY DATA ATLAS	5. TYPE OF REPORT & PERIOD COVERED Scientific. Interim.
6. PERFORMING ORG. REPORT NUMBER ERP No. 712	
7. AUTHOR(s) E.G. Mullen E.C. Whipple* H.B. Garrett, Capt, USAF D.A. Hardy, Capt, USAF	8. CONTRACT OR GRANT NUMBER(s)
9. PERFORMING ORGANIZATION NAME AND ADDRESS Air Force Geophysics Laboratory (PHG) Hanscom AFB Massachusetts 01731	10. PROGRAM ELEMENT, PROJECT, TASK AREA & WORK UNIT NUMBERS 62101F 76610803
11. CONTROLLING OFFICE NAME AND ADDRESS Air Force Geophysics Laboratory (PHG) Hanscom AFB Massachusetts 01731	12. REPORT DATE 11 August 1980 13. NUMBER OF PAGES 43
14. MONITORING AGENCY NAME & ADDRESS(if different from Controlling Office)	15. SECURITY CLASS. (of this report) Unclassified 15a. DECLASSIFICATION DOWNGRADING SCHEDULE
16. DISTRIBUTION STATEMENT (of this Report) Approved for public release; distribution unlimited.	
17. DISTRIBUTION STATEMENT (of the abstract entered in Block 20, if different from Report)	
18. SUPPLEMENTARY NOTES *University of California at San Diego, LaJolla, CA	
19. KEY WORDS (Continue on reverse side if necessary and identify by block number) Spacecraft charging Geosynchronous environment Energetic particles Space physics Electrons Ions	

20. ABSTRACT (Continue on reverse side if necessary and identify by block number)

A preliminary study of the 100 eV to ~1 MeV plasma environment encountered by the P78-2 Spacecraft Charging at High Altitudes (SCATHA) satellite during its initial operation period was conducted. Forty-four days of 10-min averages of the four moments of the electron and ion distribution functions calculated from the SC5 and SC9 energetic particle measurements were analyzed to determine occurrence frequency, local time variation, geomagnetic activity variation, and L-shell variation. The single and double Maxwellian parameters derived from the four moments were similarly analyzed. The →

DD FORM 1 JAN 73 1473 EDITION OF 1 NOV 65 IS OBSOLETE

Unclassified

SECURITY CLASSIFICATION OF THIS PAGE (When Data Entered)

2. (Cont)

interrelationships between the moments and derived parameters were computed and the results compared with the ATS-5 and ATS-6 atlas of Garrett et al. ~~(1980a, b).~~ (1980). Results of this analysis establish a baseline range for the SCATHA plasma environment.

Preface

The authors wish to thank J. Feynman and C. Pike for their careful review and comments on the manuscript. Special appreciation is expressed to F. A. Hanser of Panametrics, Inc. for discussions on the SC5 data; to R. E. McInerney of AFGL and D. E. Delorey of Boston College for computer reduction and statistical programming of the data sets; to A. H. Wendel of AFGL for developing the Maxwellian SC9 data extrapolation routine, and to A. T. Campbell and D. L. Gustafson of Boston College for producing numerous data displays so necessary for timely completion of this manuscript.

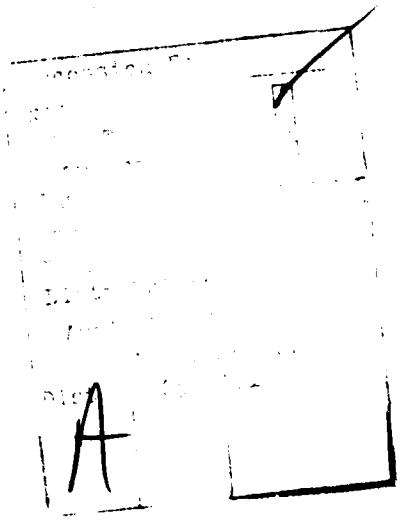

Contents

Illustrations

Tables

P78-2 SCATHA Preliminary Data Atlas

1. INTRODUCTION

The P78-2 SCATHA satellite was launched into a near-geosynchronous, equatorial orbit in January 1979. This satellite represents the culmination of five years of effort by the Air Force and NASA to provide a comprehensive means to study the effects of spacecraft charging on satellite systems. SCATHA is uniquely designed and instrumented to study the plasmas and fields in the earth's vicinity in conjunction with spacecraft charging effects.[1] Current efforts by the SCATHA principal investigators will provide detailed analyses of various "key event" periods or intervals of special interest. To supplement these studies, the Air Force Geophysics Laboratory has been tasked with the responsibility of providing a statistical atlas of the SCATHA plasma environment. The initial effort in formulating the atlas produced a statistical analysis of ~ 3000 10-min estimates (44 days) of the four moments of the 100 eV to ~ 0.5 MeV plasma measurements from the SC5 and SC9 particle detectors. This analysis is presented as a preliminary rapid-response atlas of the SCATHA plasma environment.

The results of this preliminary study will be presented in three parts. The first part will be about the data base. A brief review of the P78-2 SCATHA satellite

(Received for publication 11 August 1980)

1. Durrett, J.C., and Stevens, J.R. (1979) Description of the space test program P78-2 spacecraft and payloads, in Spacecraft Charging Technology — 1978, edited by R.C. Finke, and C.P. Pike, NASA CP-2071/AFGL-TR-79-0082, 4-10.

and the SC5 and SC9 instruments will be given. For a more detailed review of the satellite and its instrumentation, see SAMSO TR-78-24 by Stevens and Vampola.[2] As the derivation of the four moments and the associated 1 Maxwellian and 2 Maxwellian parameters have been previously discussed in the literature,[3,4] only a short summary of the variables will be given. Data constraints will also be discussed. The second part will contain the statistical results in terms of averages, standard deviations, and histograms. The data will be displayed as a function of local time, Kp, and L-shell. Scatter plots of the different parameters as functions of each other will also be displayed. The third part will compare the SCATHA data results with the ATS-5 and ATS-6 statistical results of Garrett et al[5,6] and discuss the results in terms of current understanding of the near-geosynchronous plasma environment. Appendix A is included that describes the data processing procedures used to convert the SC5 and SC9 data from counts to differential energy flux and a method for extending the effective range of the SC9 data due to energy bandpass limitations.

2. DATA BASE

2.1 Satellite

The P78-2 SCATHA satellite was launched on 30 January 1979 into a 5.5 $R_E \times 7.7$ R_E (R_E = 1 earth radius), low inclination (~ 8°) orbit. The satellite drifts eastwardly about 6° per day resulting in data sampling at approximately all local times for radial distances between 5.5 R_E and 7.7 R_E. The satellite is cylindrical in shape (~ 1.75 m in length and diameter) and has seven experimental booms. The satellite is spin stabilized at approximately 1 rpm with the spin axis of the satellite located in the orbital plane of the satellite and normal to the earth-sun line. This allows a detector on the cylindrical surface to sample all pitch angles.

2. Stevens, J.R., and Vampola, A.L. (Editors) (1978) Description of the Space Test Program P78-2 Spacecraft and Payloads, SAMSO-TR-78-24.

3. Garrett, H.B., and DeForest, S.E. (1979) Time-varying photoelectron flux effects on space craft potential at geosynchronous orbit, J. Geophys. Res. 84:2083-2088.

4. Garrett, H.B. (1979) Review of quantitative models of the 0-100 KeV near-earth plasma, Rev. Geophys. Space Phys. 17:397-417.

5. Garrett, H.B., Schwank, D.C., and DeForest, S.E. (1980a) A statistical analysis of the low energy geosynchronous plasma environment, Part I — Electrons, submitted to Planet. Space Sci.

6. Garrett, H.B., Schwank, D.C., and DeForest, S.E. (1980b) A statistical analysis of the low energy geosynchronous plasma environment, Part II — Ions, submitted to Planet. Space Sci.

2.2 Instruments

The instruments employed in this study are the Air Force Geophysics Laboratory (AFGL) SC5 Rapid Scan Particle Detector and the University of California at San Diego (UCSD) SC9 Charged Particle Experiment. Of particular concern to this study are the different energy ranges, pitch angles, and time intervals sampled by the experiments. Although an attempt was made to negate these differences in the analysis, some instrumental effects are apparent in the results.

The SC5 instrument is designed to sample the electron and ion fluxes incident on the P78-2 SCATHA satellite at ~ 1 sec time intervals over a very large energy range (~ 50 eV - 0.5 MeV). The extreme energy range necessitates a unique design involving electrostatic and solid state detectors. The energy bins for the SC5 detectors together with a description of the instrument and its calibration are contained in Hanser et al.[7] For this study, only detectors mounted parallel to the spin axis were used since these are not subject to sun pulses that occasionally affect the perpendicular detectors.

The SC9 instrument is quite similar to the UCSD electrostatic analyzers flown on ATS-5[8] and ATS-6.[9] The basic sampling time is 0.25 sec for each of 64 energy channels. There are five detectors (two electron and three ion), two pairs of which are designed to scan in a plane tangent to the cylindrical side of the spacecraft (North-South, NS) and one that scans across the top face of the spacecraft (East-West, EW). The electron and ion NS pair are the only set employed in this preliminary analysis as they covered the largest energy range (~ 1 eV to 81 keV) in logarithmically spaced bins.

2.3 Moment Calculations

In order to compute the four moments, the detector count data were first averaged over 10-min intervals and then converted to differential energy spectra as a function of time. The resulting averaged spectra were then integrated according to the following formulas to give the first four electron and ion moments:

$$ND_i = 4\pi \int_0^\infty (V^0)\, f_i\, V^2\, dV \qquad (1)$$

7. Hanser, F.A., Hardy, D.A., and Sellers, B. (1979) Calibration of the Rapid Scan Particle Detector Mounted in the SCATHA Satellite, AFGL-TR-79-0167.
8. DeForest, S.E., and McIlwain, C.E. (1971) Plasma clouds in the magnetosphere, J. Geophys. Res. 76:3587-3611.
9. Mauk, B.H., and McIlwain, C.E. (1975) ATS-6 Auroral particle experiment, IEEE Trans. Aerospace and Electronic Systems, AEA-11(No. 6):1125-1130.

$$NF_i = \int_0^\infty (V^1)\, f_i\, V^2\, dV \tag{2}$$

$$ED_i = 4\pi \int_0^\infty 1/2m\, (V^2)\, f_i\, V^2\, dV \tag{3}$$

$$EF_i = \int_0^\infty 1/2m\, (V^3)\, f_i\, V^2\, dV \tag{4}$$

where

$$f_i(E) = \frac{d(EF_i)}{dE} \quad \frac{m_i^2}{2E^2}$$

E = $1/2\, m_i\, V^2$,

m_i = mass of species i,

V = velocity,

ND_i = number density of species i (number-cm^{-3}),

NF_i = number flux for species i (number-$cm^{-2}s^{-1}sr^{-1}$),

ED_i = energy density for species i (eV-cm^{-3}),

EF_i = energy flux for species i (eV-cm^{-2}-$s^{-1}sr^{-1}$),

n_i = number density of species i,

T_i = equivalent temperature of species i,

k = Boltzmann constant.

Given that the spectra can be defined by a Maxwell-Boltzmann distribution function

$$f(V) = n_i \left(\frac{m_i}{2\pi kT}\right)^{3/2} e^{-m_i V^2/2kT}, \tag{5}$$

we can define, given Eqs. (1-4), two values of equivalent T;

$$TAVG = \frac{2}{3}\,\frac{1}{k}\,\frac{ED}{ND}, \tag{6}$$

$$TRMS = \frac{1}{2}\,\frac{1}{k}\,\frac{EF}{NF}. \tag{7}$$

If the plasma were indeed a Maxwellian, then TAVG would equal TRMS, and they would be the true temperature. This is not generally true. Instead, Garrett et al[5, 6] have shown that a representation in terms of the sum of two distributions of

the form of Eq. (5) is adequate for the electron and, to a lesser extent, the ion populations encountered by ATS-5 and ATS-6. This gives rise to two pairs of number densities and temperatures, (N1, T1) and (N2, T2), where the first set is the lower energy component. These six parameters, TAVG, TRMS, N1, T1, N2, and T2, are statistically analyzed below along with the four moments. Throughout the study, NF in (number-cm^{-2}-s^{-1}-sr^{-1}) is used interchangeably with J, the current density in nA-cm^{-2}. The conversion is:

$$J = \pi q(NF) .$$

2.4 Constraints

In using Eqs. (1) through (7), the following assumptions are made:

(1) The plasma is isotropic. SC5 data (Hardy, private communication) explicitly shows this to be untrue although for quantities averaged over a 10-min period, this effect is probably not serious.

(2) m_i is assumed to be that of H^+. Data from GEOS and preliminary data from SC8 show that the composition can vary significantly. However, there are presently few statistics on this effect although the assumption may be valid a large percent of the time.

(3) There is no spacecraft charging. For the days of this analysis, a cursory study of the spectra revealed that the spacecraft to space potential was probably near zero. This does not mean that differential potentials were not present but does indicate that satellite potential effects were likely not significant.

In addition, the following data refinements were utilized for this study:

(1) The energy ranges of the SC5 and SC9 instruments were cut off below 100 eV. This was done to provide better agreement between the spectra for the two instruments and, more importantly, to avoid the problem of contamination of the low energy electron data. Low energy photoelectrons and secondary particles trapped in the vicinity of the space vehicle cannot be unambiguously separated from the ambient electrons.

(2) The high energy cutoff of the SC9 instrument is much lower than the cutoff of SC5 (~ 80 keV as compared to ~ 0.5 MeV). To help compensate for this disparity, the SC9 data were extended to cover the range up to 100 keV by assuming a Maxwell-Boltzmann distribution (see Appendix A for method). Even with the extended energy range, the SC9 data still do not cover the high energy range of SC5 so that the SC5 high energy temperature estimates are in general 50 percent to 100 percent higher. The SC9 data are in general limited to plasma temperatures of 25 keV or less.

2.5 Data Base Selection

In this preliminary analysis of the SCATHA environment, data from the entire first year of SCATHA operations were inspected, and only those days for which simultaneous SC5 and SC9 operations existed were selected. The forty-four days chosen are listed in Table 1. The data were further reduced to ~ 3000 10-min averages by the dual requirements of data quality (visual inspection) and simultaneous 10-min sampling intervals.

The final distribution of points are listed in Tables 2, 3, and 4 in terms of local time, L-shell and Kp. As should be clear from these tables, the data are limited to $Kp \leq 5_+$, and $5.5 \leq L \leq 8.5$, and biased to the 06 to 12 LT regimes. The sampling bias in the data set does in some cases affect the results, so care must be taken in interpretation of the statistical graphs. The Kp limits will necessitate extending the data base for the final atlas to periods when Kp is on the average much higher to adequately study the geomagnetic variations. The L-shell data are sufficiently confined in radial distance to be compared to the ATS-5 and ATS-6 data.

Table 1. AFGL Preliminary Atlas Days

1979 Day of Year	1979 Day of Year
40 thru 47	162
50	164
52 thru 57	166
77-78	168
121	170
123	172
125	174
140	178
142	194
144	200
146	202
152	204
154	206
156	208
158	212
160	

Table 2. Data Base: Local Time vs L-shell

LOCAL TIME	Total	375	250	454	611	667	352	111	2920
	21-24	59	18	6	17	75	94	52	321
	18-21	81	16	53	76	42	22	0	290
	15-18	38	65	11	0	0	10	10	134
	12-15	61	42	85	18	1	0	4	211
	9-12	75	46	77	184	59	0	0	441
	6-9	56	96	66	109	319	5	0	651
	3-6	0	4	109	196	145	70	7	531
	0-3	5	63	47	11	26	151	38	341
		5.5	6.0	6.5	7.0	7.5	8.0	8.5	Total

L-Shell

Table 3. Data Base: Kp vs L-shell

Kp	Total	375	250	454	611	667	352	111	2920
	5+	10	14	6	17	37	0	4	88
	4+	57	31	35	38	96	32	3	292
	3+	119	88	83	107	139	81	30	647
	2+	100	99	155	205	171	117	41	888
	1+	57	69	108	159	121	85	19	618
	0+	32	49	67	85	103	37	14	387
		5.5	6.0	6.5	7.0	7.5	8.0	8.5	Total

L-Shell

Table 4. Data Base: Kp vs Local Time

Kp	Total	341	531	651	441	211	134	290	320	2920
	5+	3	22	28	5	1	1	13	15	88
	4+	31	46	77	51	9	22	37	19	292
	3+	90	105	116	86	57	23	76	94	647
	2+	110	161	192	155	76	32	68	94	888
	1+	81	129	138	99	14	21	68	68	618
	0°	26	68	100	45	54	35	28	31	387
		00-03	03-06	06-09	09-12	12-15	15-18	18-21	21-24	Total

Local Time

3. STATISTICAL DATA ANALYSIS

3.1 Introduction

Standard statistical techniques which proved to be useful scientific methods for studying the ATS-5 and ATS-6 data were employed to analyze the average variations in the SCATHA near-geosynchronous plasma environment. Specifically, variations in terms of local time, geomagnetic activity, and radial distance were determined by averaging the data in, respectively, 3-hr local time bins, Kp intervals, and L-shells. Complex interrelationships between pairs of parameters were studied by means of scatter plots. The results of these techniques are discussed in this section.

3.2 Averages and Histograms

The most basic information available in a data set are the average values and the occurrence frequencies of the values. Averages and standard deviations of the four moments, ND, NF (or J), ED and EF together with the derived quantities are listed in Tables 5 and 6 for SC5 and SC9 respectively (Note: the SC9 data have all been corrected for the finite bandwidth effect—see Appendix A). Occurrence frequency histograms of the moments are plotted in Figure 1a; TAVG, TRMS, T1 and T2 in Figure 1b; and N_1 and N_2 in Figure 1c.

As can be seen in Figures 1a, 1b, and 1c, the electron data are not well represented by a Gaussian distribution; therefore, the standard deviation as given in Tables 5 and 6 and is not a particularly useful quantity. The situation is somewhat improved for the ions but the standard deviation should still be considered circumspectively.

Except for the temperatures, the histograms for SC5 and SC9 are in good agreement. The SC6 temperatures are consistently higher than the SC9 values by as much as ~ 100 percent. This is readily attributed to the different energy cutoffs

(100 keV as opposed to 0.5 MeV) for the two instruments. The results for the moments and derived quantities are qualitatively similar; that is, the temperatures are much more Gaussian than the other parameters implying that the greatest variations are in number density and not in temperature or particle mean energy.

Table 5. SCATHA SC5 Particle Statistics

Parameter	Electrons		Ions	
	Average	S. D.	Average	S. D.
ND (cm^{-3})	0.823	$\pm$ 0.753	0.690	$\pm$ 0.406
J($nA\text{-}cm^{-2}$)	0.086	$\pm$ 0.084	4.14×10^{-3}	$\pm 2.57 \times 10^{-3}$
ED ($eV\text{-}cm^{-3}$)	3.24×10^{3}	$\pm 3.3 \times 10^{3}$	1.24×10^{4}	$\pm 8.86 \times 10^{3}$
EF ($eV\text{-}cm^{-2}\text{-}s^{-1}\text{-}sr^{-1}$)	2.26×10^{12}	$\pm 2.29 \times 10^{12}$	2.93×10^{11}	$\pm 2.51 \times 10^{11}$
TAVG (keV)	3.20	$\pm$ 2.67	12.1	$\pm$ 5.17
TRMS (keV)	8.26	$\pm$ 5.81	16.8	$\pm$ 7.10
N1 (cm^{-3})	0.654	$\pm$ 0.603	0.330	$\pm$ 0.242
N2 (cm^{-3})	0.169	$\pm$ 0.225	0.360	$\pm$ 0.241
T1 (keV)	0.725	$\pm$ 0.662	2.13	$\pm$ 1.44
T2 (keV)	17.4	$\pm$11.0	21.1	$\pm$ 8.68

Table 6. SCATHA SC9 Particle Statistics*

Parameter	Electrons		Ions	
	Average	S. D.	Average	S. D.
ND (cm^{-3})	1.09	$\pm$ 0.890	0.579	$\pm$ 0.345
J($nA\text{-}cm^{-2}$)	0.115	$\pm$ 0.098	3.32×10^{-3}	$\pm 2.08 \times 10^{-3}$
ED ($eV\text{-}cm^{-3}$)	3.71×10^{3}	$\pm 3.44 \times 10^{3}$	9.44×10^{3}	$\pm 6.82 \times 10^{3}$
EF ($eV\text{-}cm^{-2}\text{-}s^{-1}\text{-}sr^{-1}$)	1.99×10^{12}	$\pm 2.03 \times 10^{12}$	2.01×10^{11}	$\pm 1.71 \times 10^{11}$
TAVG (keV)	2.49	$\pm$ 1.48	11.2	$\pm$ 4.55
TRMS (keV)	4.83	$\pm$ 2.89	14.5	$\pm$ 5.27
N1 (cm^{-3})	0.780	$\pm$ 0.701	0.191	$\pm$ 0.162
N2 (cm^{-3})	0.310	$\pm$ 0.368	0.388	$\pm$ 0.257
T1 (keV)	0.550	$\pm$ 0.316	0.804	$\pm$ 1.04
T2 (keV)	8.68	$\pm$ 4.02	15.8	$\pm$ 5.02

*Extended assuming a Maxwell-Boltzmann Distribution.

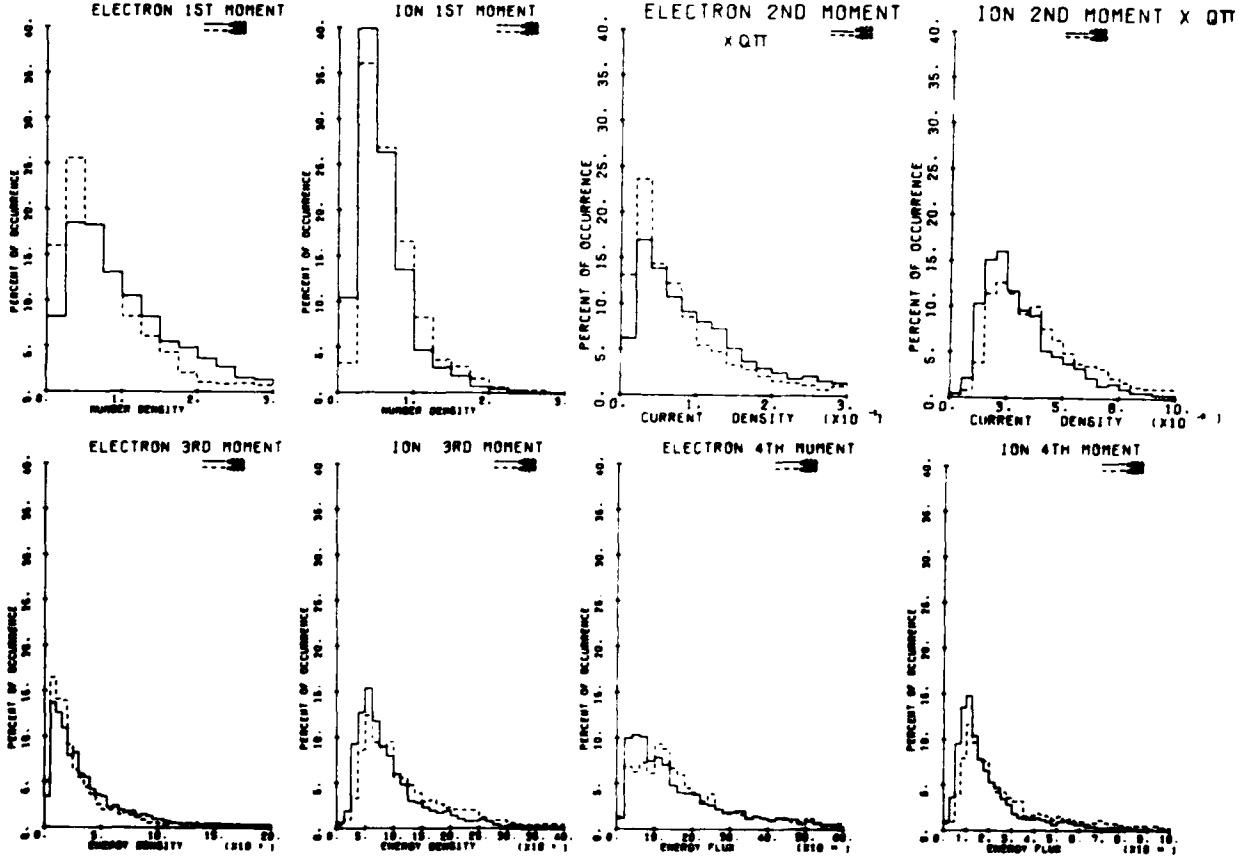

Figure 1a. Histograms of the Percent of Occurrence of the First Four Moments of the Electron and Ion Distribution Functions as Calculated From the SC5 and SC9 Energetic Particle Measurements Aboard the SCATHA Satellite. (Number density is in number cm^{-3}. Current density is in $nA\text{-}cm^{-2} \times 10^{-1}$ for electrons and $\times 10^{-3}$ for ions. Energy density is in $eV\text{-}cm^{-3} \times 10^{3}$. And, energy flux is in $eV\text{-}cm^{-2}\text{-}s^{-1}\text{-}sr^{-1} \times 10^{11}$)

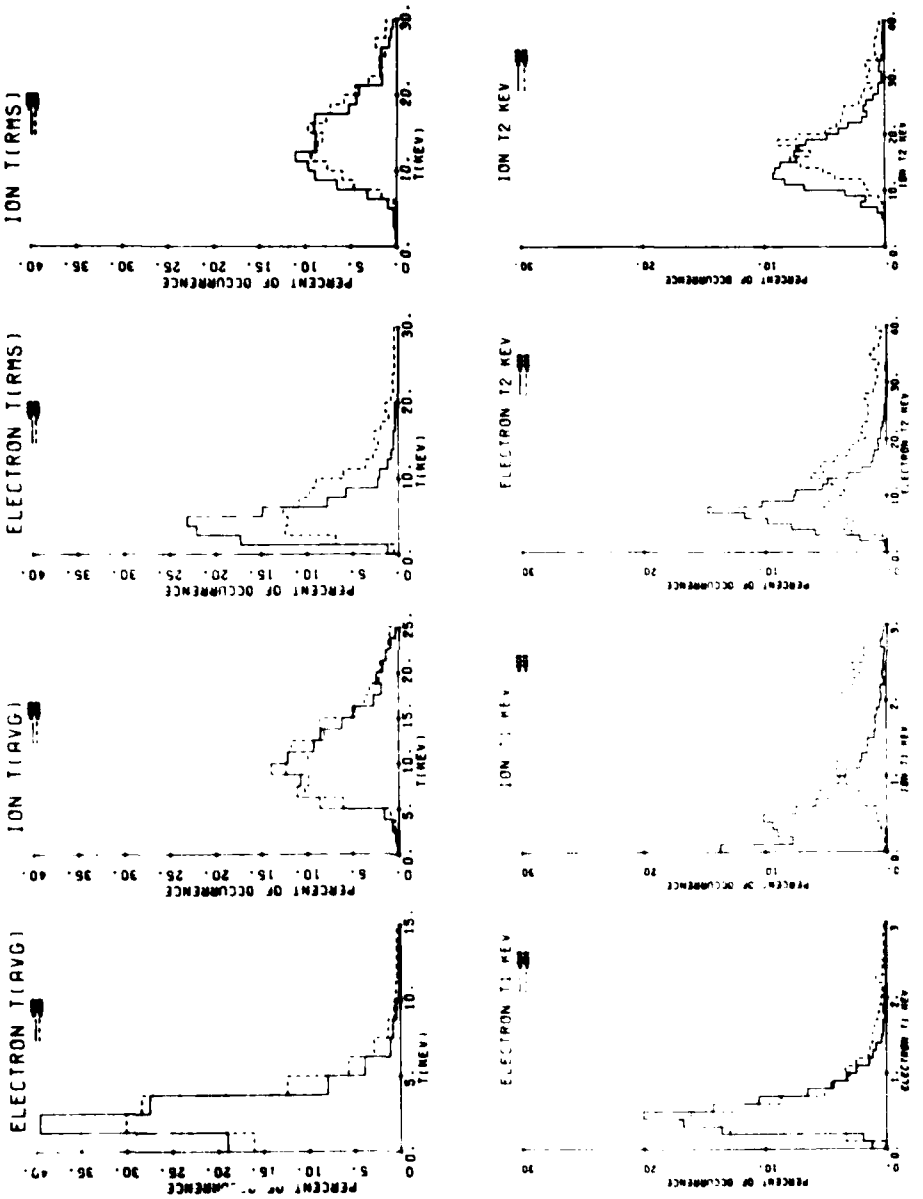

Figure 1b. Histograms of the Percent of Occurrence of the Calculated Temperatures TAVG, TRMS, T1 and T2 in keV From the SC5 and SC9 Energetic Particle Measurements

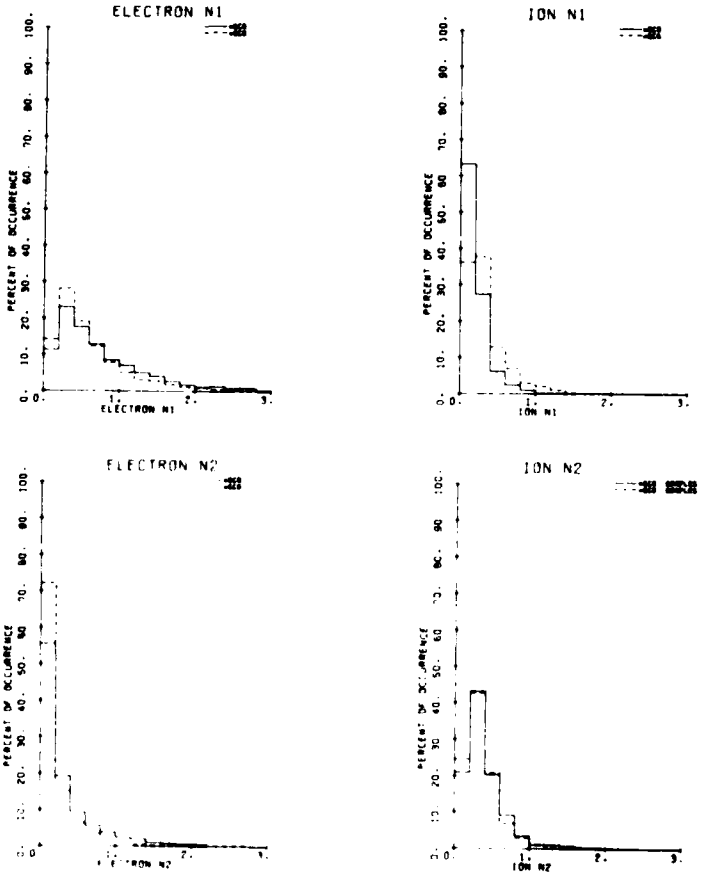

Figure 1c. Histograms of the Percent of Occurrence of the Calculated 2 Maxwellian Number Densities N1 for the Lower Energy Population and N2 for the Higher Energy Population in Number cm^{-3}

3.3 Local Time Variations

Pronounced asymmetries in local time (that is, satellite ground track position relative to the sun) exist in the near-earth plasma environment. In order to study this variation in the SC5/SC9 data, 10-min values were averaged in 3-hr local time bins. The results are plotted in Figures 2a, 2b, 2c, 3a and 3b.

The SC5 and SC9 local time moment variations are in excellent agreement considering instrumental differences. Figures 2a and 2b indicate large local time variations in the electron moments of the order of four times the minimum values. For Kp values 5+ or greater, this local time variation can exceed a factor of ten. Although the data base is biased as can be seen in Tables 2, 3 and 4, for the range of Kp and L-shell values used in this study, the electron moments are minimum and nearly constant in the 1200 to 1800 local time range and peak and show maximum variation in the 0000 to 0600 local time range independent of Kp or L-shell. The ion moments on the other hand are much less structured with local time with no definitive variation with local time identifiable from this study. N_1 and N_2 (Figure 3a) exhibit the same behavior as the moments for both the electrons and the ions.

The SC5 and SC9 temperature variations with local time, Figures 2c and 3b, are not in as good agreement as the other parameters. Although TAVG, TRMS, and T2 are in agreement phasewise, they are only in quantitative agreement near midnight when all are minimum. This is likely a reflection of the energy band-pass differences of the detectors. The differences in T1 between SC5 and SC9 are quite large and are due to the low energy cutoff of the SC5 detectors which can be seen for the ions in Figure 4 and will be discussed further below. Assuming the SC9 T1 values to be correct, the local time variations in the low energy T1 component temperatures are out of phase with the high energy T2 components, with T2 values peaking between 1200-1800 L.T, and T1 values having a minimum in the same time interval.

3.4 Variations With Geomagnetic Activity

Variations in geomagnetic activity have been studied by averaging the data in Kp bins. The results are plotted in Figures 2 and 3 for both the ions and electrons. Although Kp (or equivalently ap) is not necessarily the best indicator of geomagnetic activity, it is the most readily available and currently used by the Air Weather Service in most of its activities.

The increases in the SC5 and SC9 moments with Kp for both the electrons and ions are in good agreement. The electron results are, in fact, in excellent quantitative agreement between the two data sets. When studied in terms of temperature and N1 and N2, the increases with Kp are evident in N1 and N2. The temperatures show little consistent variation with Kp < 4+; however, there is some evidence in the data for Kp > 5+ a pattern may exist. The lack of sufficient high Kp values in the 1200-2100 and 0000-0300 local time bins biases the data base sufficiently to preclude any definitive results.)

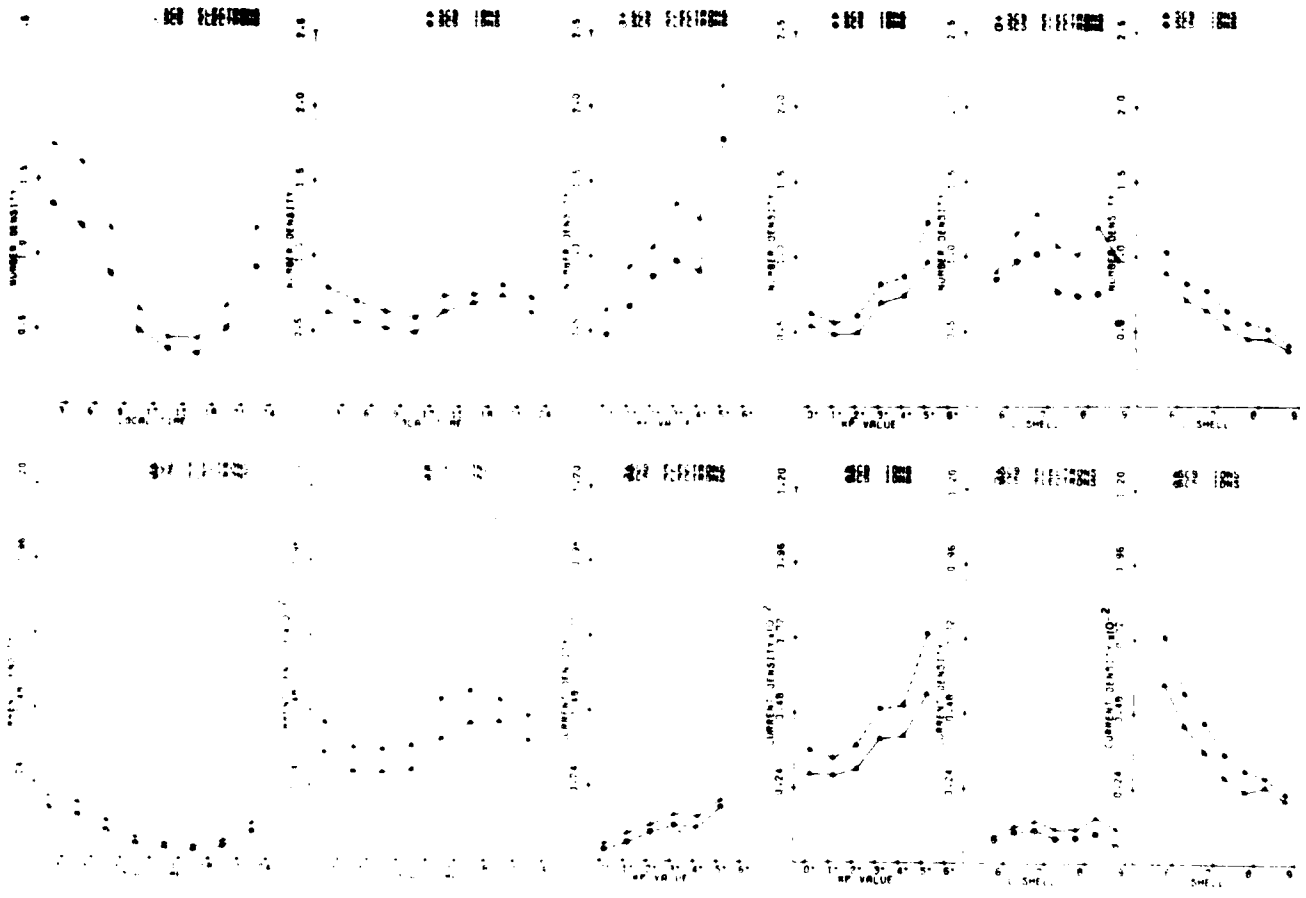

Figure 2a. SC5 and SC9 Number Density and Current Density Moment Variations With Local Time, Kp and L-shell. (Number density is in number cm^{-3}, and current density is in $nA\text{-}cm^{-3}$)

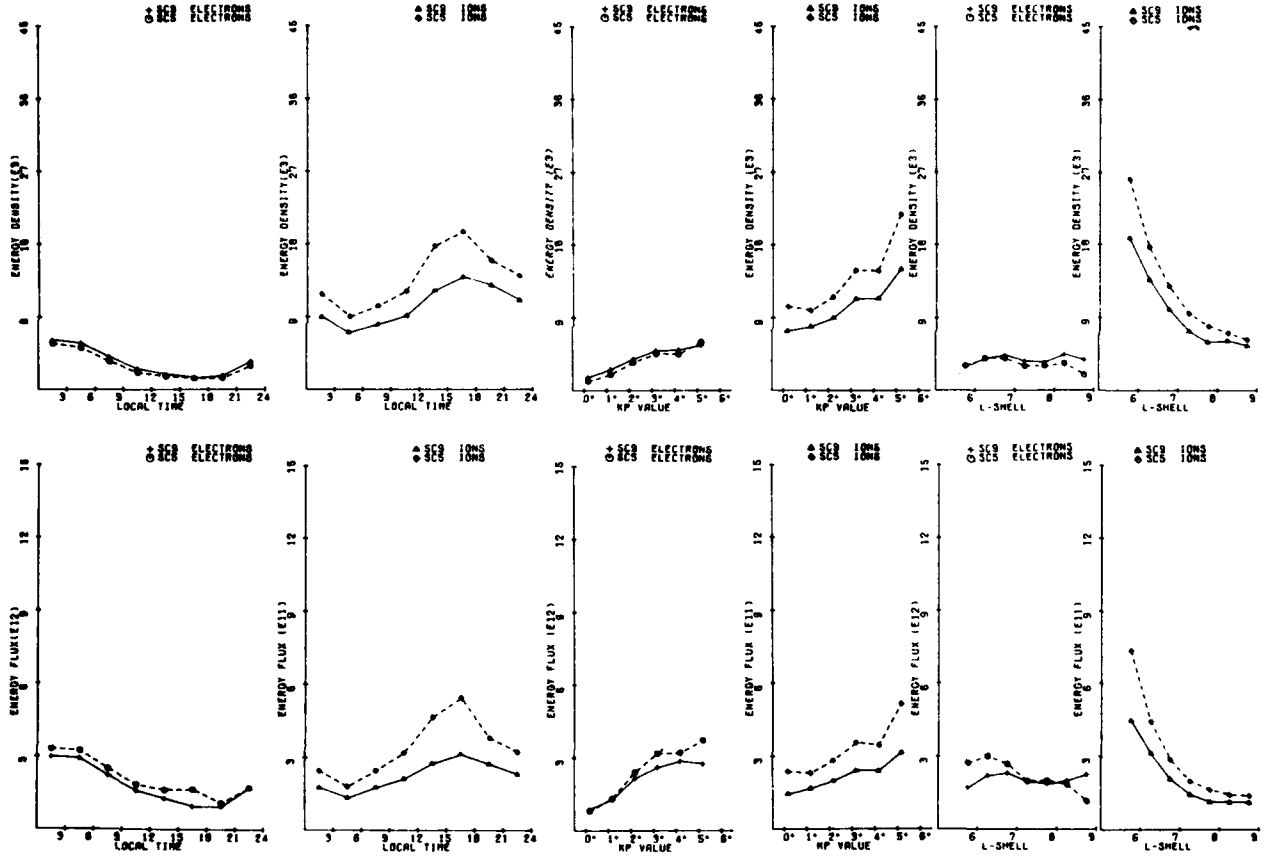

Figure 2b. SC5 and SC9 Energy Density and Energy Flux Moment Variations With Local Time, Kp and L-shell. (Energy density is in eV-cm^{-3} × 10^{3}, and energy flux is in eV-cm^{-2}s^{-1}-sr^{-1} × 10^{12} for electrons and × 10^{11} for ions)

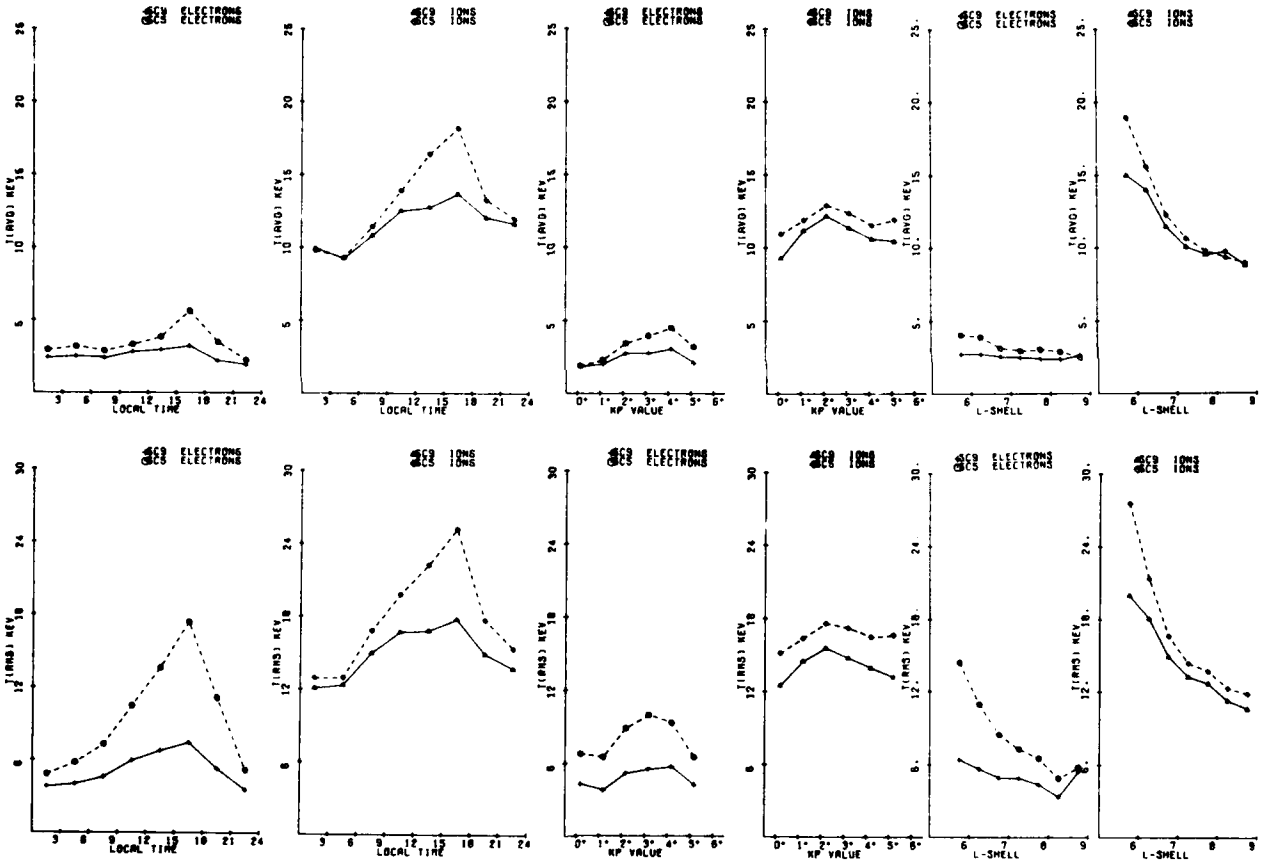

Figure 2c. SC5 and SC9 TAVG and TRMS Variations With Local Time, Kp and L-shell. (TAVG and TRMS are in keV)

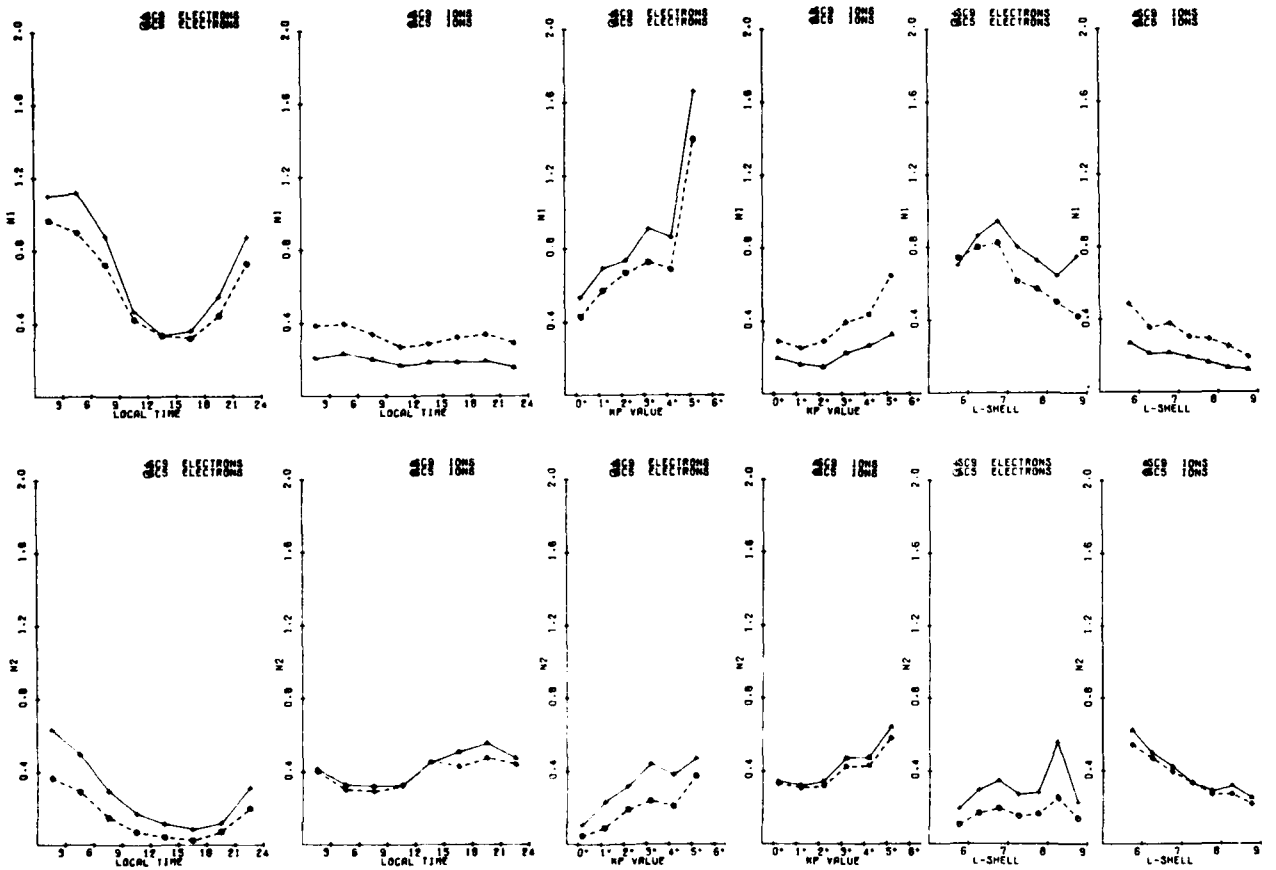

Figure 3a. SC5 and SC9 2 Maxwellian Temperatures T1 and T2 (in eV × 10^3) Variations With Local Time, Kp and L-shell

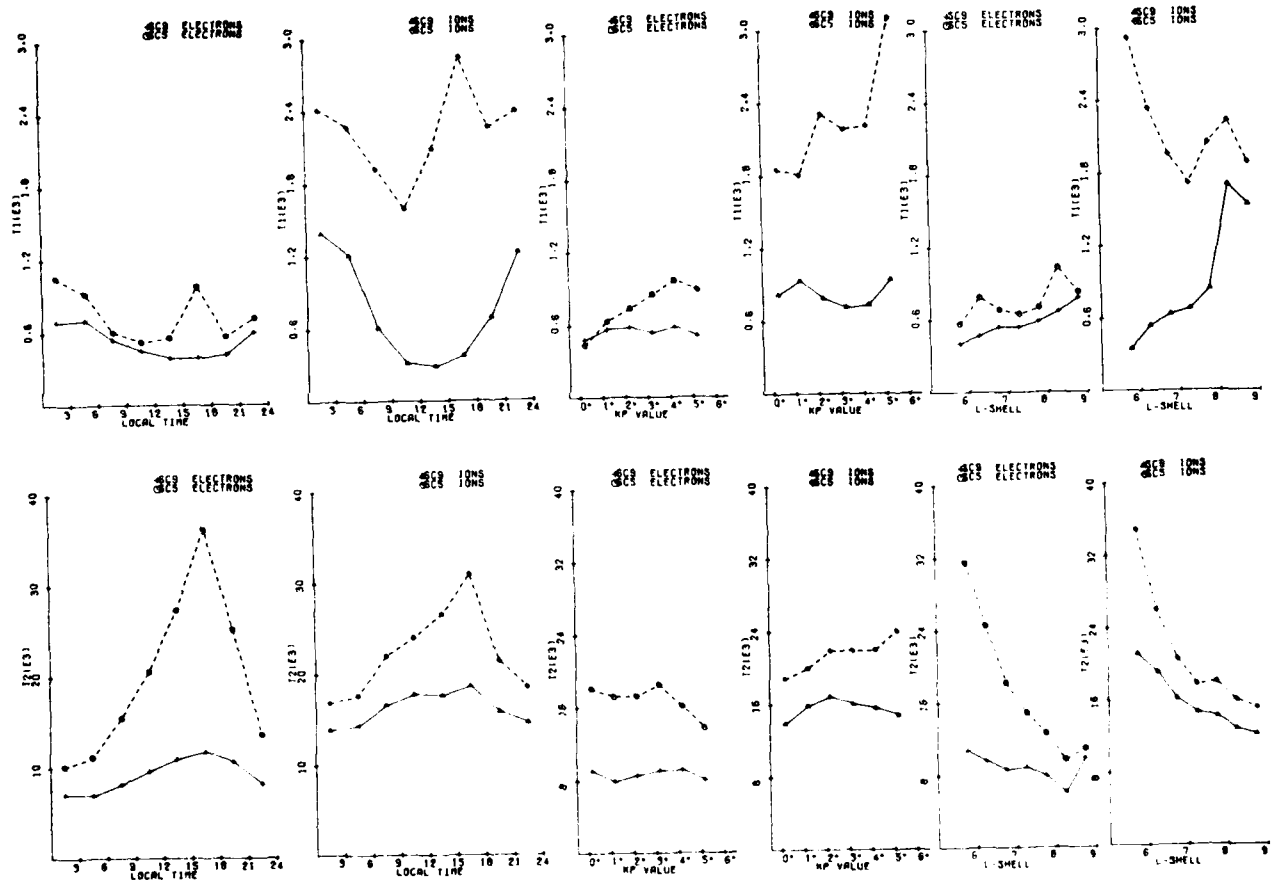

Figure 3b. SC5 and SC9 2 Maxwellian Temperatures T1 and T2 (in eV × 10^3) Variations With Local Time, Kp and L-shell

3.5 Variations With L-shell

The variation with radial distance or L-shell (that is, the normalized radial distance in terms of the earth's magnetic field) of the near-earth plasma is a well known phenomenon.[10] In order to study this effect, the P78-2 SCATHA orbital elements were first converted to L coordinates using the Olsen-Pfitzer model of the earth's magnetic field. The data were then averaged in terms of 0.5L bins between L=5 and 8.5. The results are plotted in Figures 2 and 3.

The most striking feature evident in the L-shell plots is the pronounced increase in all of the ion moments with decreasing L and the seeming lack of a consistent variation in the electron moments with L value. However, when the electron moments are analyzed only in the 0000-0300 local time range where the maximum variations occur, a marked peak at L=6.5 for all four moments is evident. The large magnitude variation in the ion data could bias the statistical analysis of the local time and Kp variations. This is not the case for the Kp variations. However, the ion local time variation peak between 1500 and 2100 LT may be due in part to L-shell bias since the 1500-1800 LT data is highly biased toward lower L shells, and, as mentioned previously, these peaks are not significant when careful examination of the data is performed.

When the data are plotted in terms of the temperatures and two Maxwellian parameters, most of the ion increase with decreasing L-shell is in the high energy components. N2 exhibits the largest variation in the 2100 to 0300 LT frame, while T2 and TRMS exhibit the largest change in the 0600 to 1200 LT frame. The ion T1 temperature, assuming SC9 to be correct, shows an increase with increasing L shell. This out of phase pattern is similar to that found for the T1 local time variation. For the electrons, no significant trend is evident in the data. The data can thus be partly explained in terms of a sharply defined high energy ion boundary between 5.5 and 8.5 L with increasing ion energy and density for decreasing L. As will be discussed, this may reflect an encounter with the ion ring current at the lower L-shell values.[10]

3.6 Intercomparisons of Parameters

A particularly useful method of statistically analyzing the near-earth plasma is the scatter plot. A number of pairs of plasma parameters were plotted vs each other for both SC5 and SC9. As the different parameters are not randomly correlated, pronounced relationships emerge from such a procedure that may have physical significance. For example, a slope of unity on a plot of ED vs ND or EF vs NF would correspond to an isotherm [see Eqs. (6) and (7)].

10. Frank, L. A. (1971) Relationship of the plasma sheet, ring current, trapping boundary, and plasma pause near the magnetic equator and local midnight, J. Geophys. Res. 76:2265-2275.

Figures 4 through 9 contain scatter plots for the SC5 and SC9 data. These have been selected from a number of combinations since they are representative of the types of variations observed. The figures are arranged as follows: ion 2 Maxwellian temperatures T1 vs T2, Figure 4; Moment intercomparisons, Figures 5 and 6; 2 Maxwellian component intercomparisons, Figures 7 and 8; and SC5 electron moments vs TRMS, Figure 9. Each set will be discussed in turn below.

Figure 4 shows the 2 Maxwellian parameters T1 and T2 for the ions. The purpose of this plot is to illustrate the major difference between the SC5 and SC9 results. As should be clear from this figure, T1 for the SC5 ion observations does not go below ~ 500 eV. The maximum value of T2 is lower for SC9 than SC5. The reasons for these two effects are, as discussed in an earlier section, differences in the energy ranges of the detectors. The low energy cutoff on SC5, although set at 100 eV, is often higher as the counts can be ~ 0 in the lowest ion channels for quiet geomagnetic conditions. The high energy cutoff on SC9 is significantly lower than the SC5 (100 keV vs 0.5 MeV). This effect should be kept in mind in the rest of the discussion. It mainly affects T1 and T2 for the ions.

Figures 5 and 6 are plots of ED vs ND and EF vs NF. Both qualitatively and quantitatively, the figures are very similar for SC5 and SC9. For example, the EF vs NF ion plots demonstrate a relationship of the form $EF \propto NF^{5/3}$. Much of the discussion concerning such relationships and the adiabatic relationships that they imply can be taken directly from Garrett et al.[5,6]

Given that the moment scatter plots for SC5 and SC9 are similar to the ATS-5 and ATS-6 results, Figures 7 and 8 compare the 2 Maxwellian parameters where the pairs N1 vs N2, T1 vs N1, and T2 vs N2 have been plotted for the electrons and ions. The agreement between the SC5 and SC9 data (except for the T1 effect discussed earlier) is again good. The ions do not demonstrate any pronounced interrelationships between the parameters. The discussion of these observations again follows that of the ATS-5/ATS-6 studies.

The final set of scatter plots shows the relationships between TRMS and the four moments for the SC5 electrons (Figure 9). There is a power-law relationship between these parameters which varies from an inverse relationship for (ND vs TRMS) to a direct relationship for (EF vs TRMS). This same effect is seen in the SC9 data and for TAVG.

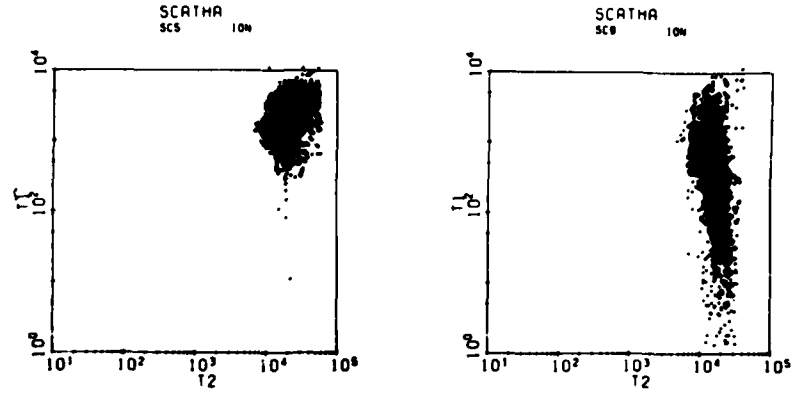

Figure 4. Scatter Plots of SC5 and SC9 2 Maxwellian Ion Temperatures T1 vs T2 in eV for the Data Set Used in the Preliminary Atlas. (The low energy T1 cutoff of SC5 and the high energy T2 cutoff of SC9 are quite evident)

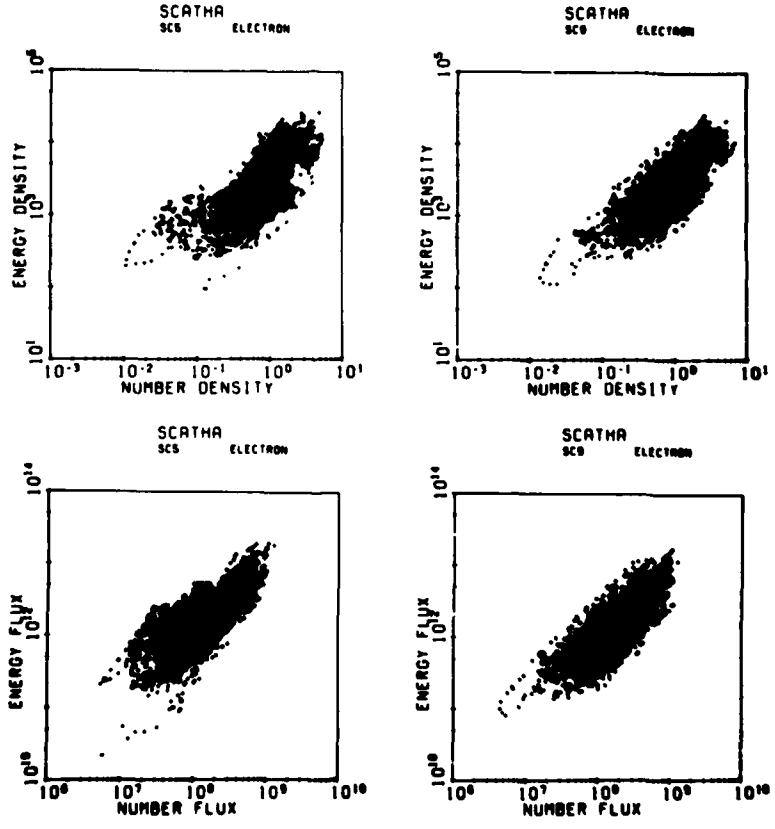

Figure 5. Scatter Plots of SC5 and SC9 Electron Moments Energy Density vs Number Density and Energy Flux vs Number Flux

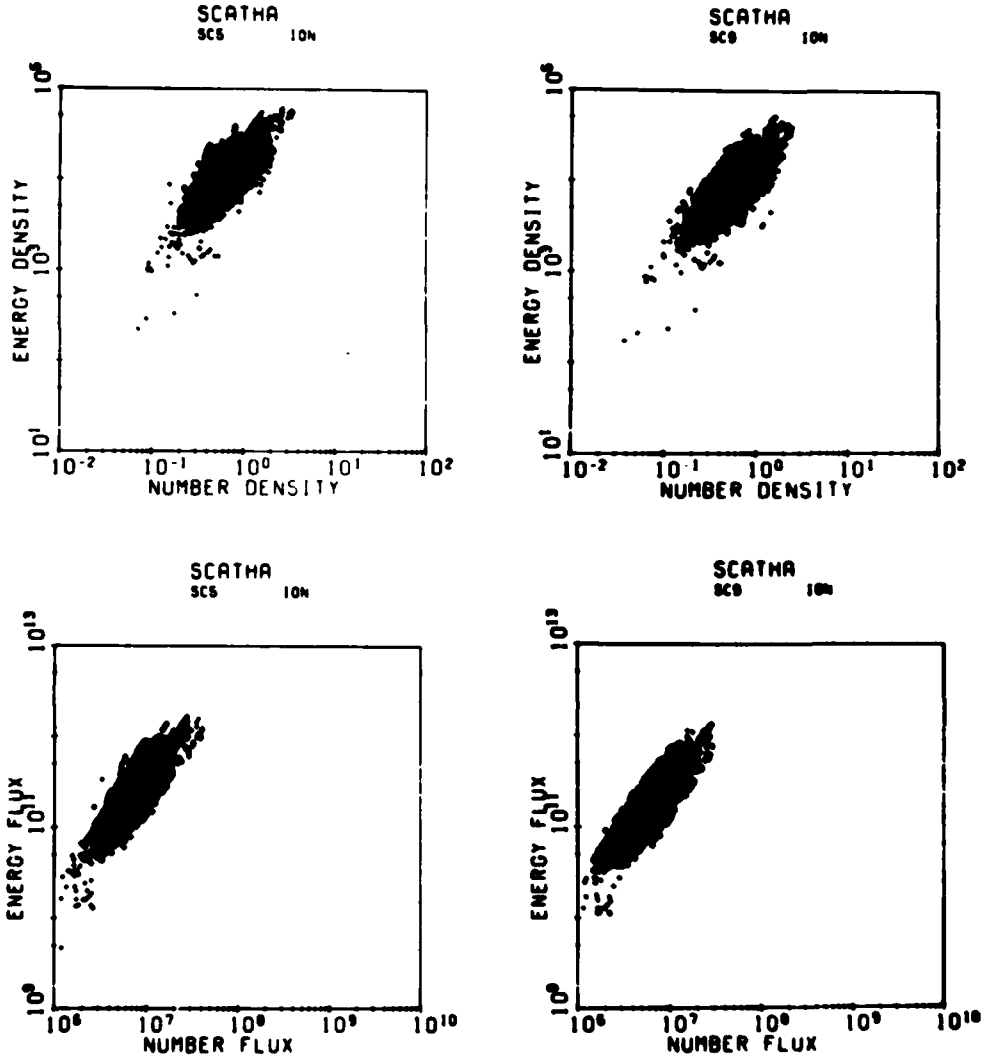

Figure 6. Scatter Plots of SC5 and SC9 Ion Moments Energy Density vs Number Density and Energy Flux vs Number Flux

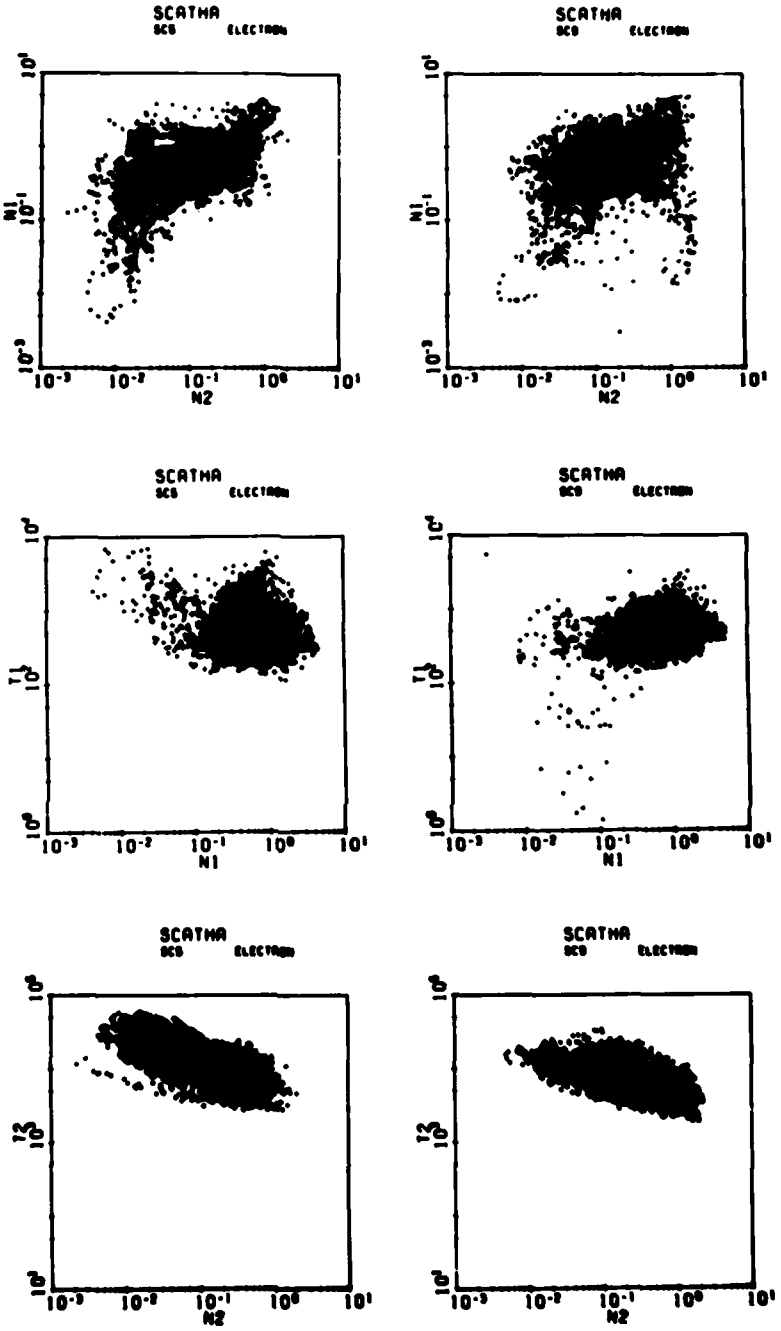

Figure 7. Scatter Plots of SC5 and SC9 2 Maxwellian Electron Values N1 vs N2, T1 vs N1, and T2 vs N2

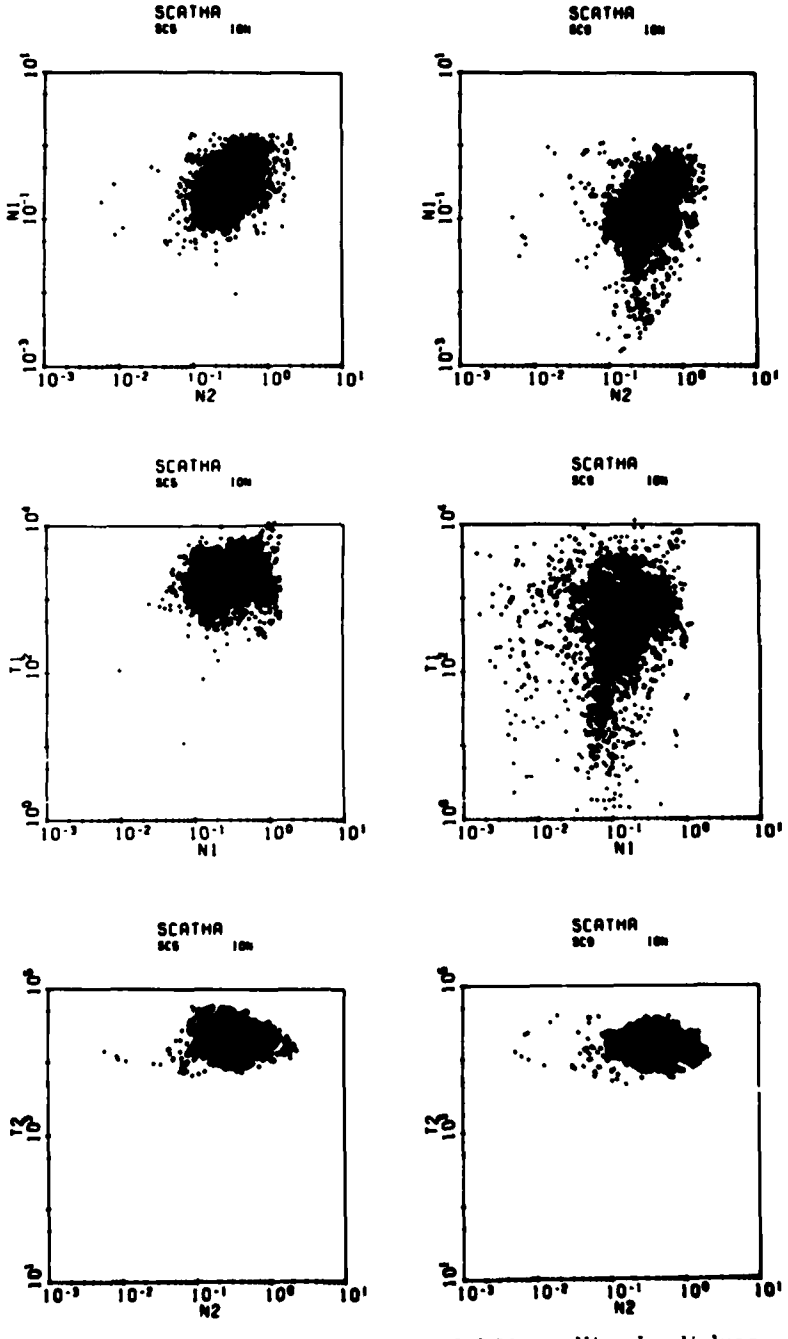

Figure 8. Scatter Plots of SC5 and SC9 2 Maxwellian Ion Values N1 vs N2, T1 vs N1, and T2 vs N2

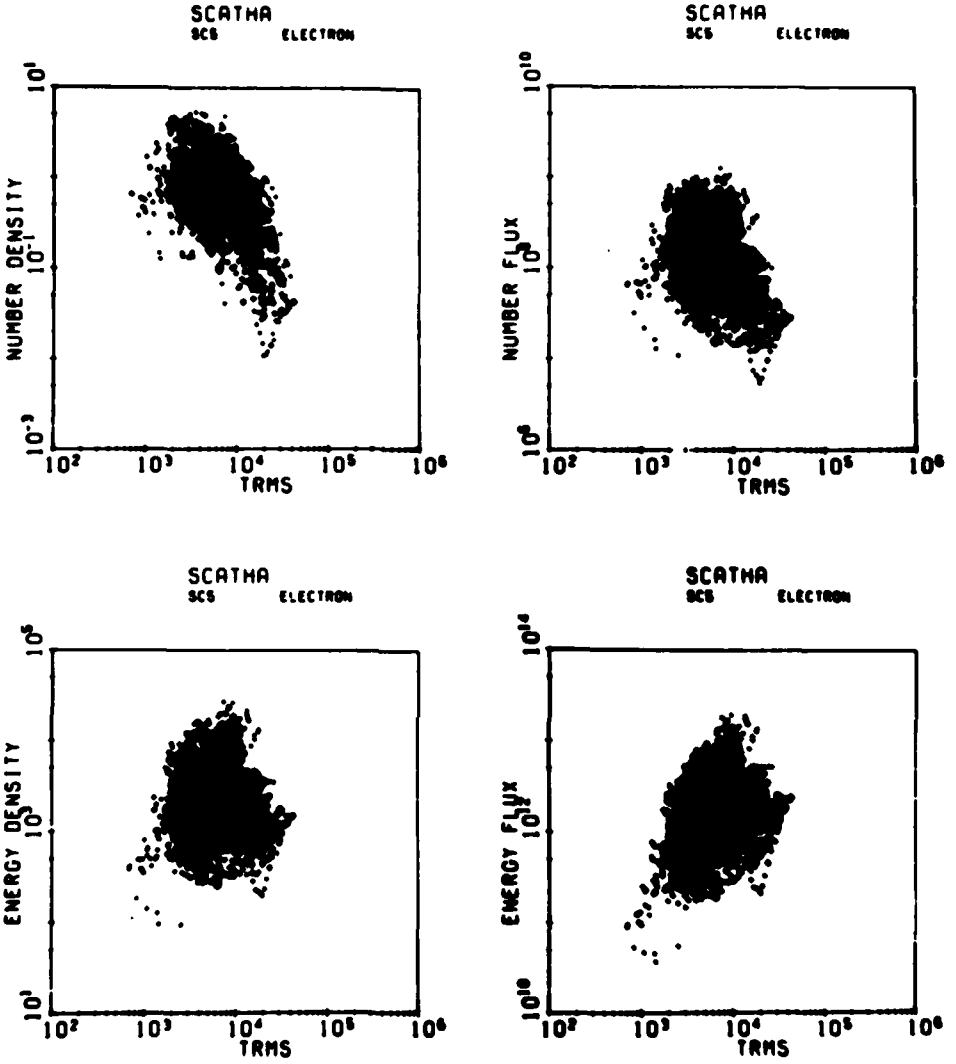

Figure 9. Scatter Plots of SC5 Electron Moments vs TRMS

4. DISCUSSION

4.1 Introduction

A major finding of this preliminary atlas is that the SC5 and SC9 statistical results are similar to the ATS-5/ATS-6 results when proper consideration of the differences in energy ranges is made. The SC5/SC9 average data, except for N1 and T1 for the ions, fall well within the ranges established by ATS-5/ATS-6. The ATS-5/ATS-6 low energy ion cutoffs were lower than the SC5/SC9 cutoffs so that the disagreement between the low energy N1 and T1 values is expected. The local time asymmetries in the near-earth plasma electron environment seen by SC5/SC9 were also clearly visible in the ATS-5/ATS-6 data. However, the high energy T2 electron component peak in the SC5/SC9 data was not readily apparent in the ATS-5/ATS-6 data where T2 showed little variation in local time. The electron results with Kp are in excellent quantitative agreement between the two data sets while the ion data from ATS-5/ATS-6 show about half the increase of the SC5/SC9 data with Kp. As ATS-5 and ATS-6 were geosynchronous satellites, no significant L-shell variations were seen. Similar scatter plot relationships were also observed in the ATS-5/ATS-6 results. Since the SCATHA and ATS-5/ATS-6 data results are statistically so comparable, the simple explanation of results in terms of current understanding of the geosynchronous environment as developed in the ATS-5/ATS-6 papers can be adopted here. A brief recapitulation of the explanation is given below followed by its application to the SCATHA statistical observations.

4.2 Geosynchronous Environment Characterization

Results from the ATS-5/ATS-6 studies showed that the geosynchronous environment can be roughly characterized by two main features. First, the near-earth plasma can be described in terms of a limited number of plasma populations which are superimposed on each other. Second, these populations change with time so as to follow specific adiabatic-like or power-law relationships. The different populations found in the ATS-5/ATS-6 studies are discussed below.

The conventional picture of the magnetosphere in the equatorial plane is of two principal regimes—the plasmasphere is close to the earth ($< 3\text{-}6\ R_E$) and the plasma sheet farther out. Due to spatial asymmetries and temporal variations of these regions, they alternately pass over the geosynchronous orbit. As the plasma sheet at geosynchronous orbit is characterized by electron densities of $\sim 1\ cm^{-3}$ and temperatures of 1-10 keV and the plasmasphere by densities of $10^1\text{-}10^4\ cm^{-3}$ and a temperature of ~ 1 eV, a geosynchronous satellite experiences extreme fluctuations in plasma conditions. As SCATHA has a radial velocity relative to these boundaries, it will typically see even more pronounced changes.

Of additional interest to this study are two other features—the outer boundary of the high energy, trapped electrons (E > 40 keV) defined by Frank[10] and the inner edge of the plasma sheet called the ion ring current (5 keV-100 keV ions circulating on trapped orbits around the earth). A final feature to take into account is the injection event, or rapid earthward movement of plasma sheet particles in the midnight sector in conjunction with increased geomagnetic activity. It is this latter event which is often associated with satellite charging.

Taking the ATS-5 and ATS-6 results into account, we can define the following populations that are visible in the data:

Electrons:

(1) Population 1: A low energy, low density population observed at all local times, except near midnight, following an injection event. This population, identified with (N1, T1), may be the residual plasma sheet electrons at low energies following a prolonged period of quiet, or the high energy end of the plasmasphere electron spectrum. It appears in the SC5/SC9 data as densities below ~ 1 cm^{-3} and T1 > 1 keV (Figure 7).

(2) Population 2: A high energy, low density population visible at all local times. It varies little in temperature (T2) with Kp, whereas its number density (N2) varies directly with Kp (Figure 3). N2 and T2 are inversely related ($T2 \sim N2^{-1/4}$) (Figure 7). This population is probably the trapped high energy electron population.

(3) Population 3: With plasma injection the number density rises in the midnight sector above ~ 1 cm^{-3} in the moderate energy range (1-20 keV). This is believed to be fresh plasma sheet particles moving in towards the earth. When this population appears, Population 1 apparently disappears. This sudden appearance of a high density, moderate energy plasma at midnight accounts for the peak in the N1 and N2 plots (Figure 3a) and the increases in the moments with Kp as this population follows an adiabatic power law where $T1 \propto N1^{1-2}$. Population 3 is not seen at noon.

Ions:

(1) Plasmasphere ions: A cold 1 to 30 eV, high density (~ 10 cm^{-3}) population is visible in the ATS-6 data. This population is also present in the SC9 data, but due to our truncation of the spectra at 100 eV, it does not appear in the data presented here. It should be carefully studied, however, if a complete statistical base is to be prepared.

(2) Ring current ions: This is a hot, trapped ion component. It closely resembles the plasma sheet fluxes so that it is difficult to identify unambiguously in our data. According to Frank,[10] however, the ring current, which generally straddles the geosynchronous orbit or is earthward of it, has a higher energy density than the plasma sheet. This can be used to distinguish, on the average, between the two regions.

4.3 SCATHA Results

Coupled with the concept of an injection event, most of the SC5/SC9 data can be explained in terms of the populations described above. In this section, a brief attempt will be made to do this. As the two Maxwellian breakout of the data is somewhat more concise, the data will be explained in terms of variations in this population.

The quiet time magnetosphere in this model is depicted as an asymmetric plasmasphere consisting of a high density, cold electron and ion population. The plasmasphere bulge is in the dusk quadrant. Superimposed on the plasmasphere are the high energy trapped electrons and, between 4 and 8 L, the hot plasma sheet with 1-20 keV particles and moderate (1-2 cm^{-3}) densities. This region is closest to the earth at midnight.

SCATHA orbits in local time move back and forth across these populations. Because of the 100 eV data cutoff, it does not see the plasmasphere particles. It does see the trapped electrons (Population 2) and the ring current ions. These go to make up N2 and T2. During quiet times it also sees a low energy residual electron (Population 1) and ion population. Since these populations drift differently, their local time variations are not equal. High energy ions are known to penetrate closer in the 1800 to 0000 LT quadrant, electrons in the 0000 to 0600 LT quadrant. Moving in radially, SCATHA goes from the hot plasma sheet to a hotter ring current, so that the ion moments increase with decreasing L-shell (Figures 2 and 3).

The active magnetosphere is somewhat different than the quiet magnetosphere; that is, during an injection event, hot plasma sheet particles move earthward, increasing the density of the moderate energy particles. This cloud of particles rapidly disperses away from midnight. This influx is so large as to increase all the moments as observed in the data. The increase in density occurs for both N1 and N2 so that, for the electron Population 2, T2 drops slightly. For the electrons, the increase in the moments with Kp and the near constancy of the temperatures is thus explained. For the ions the change from the hot, low density ring current to the hot, high density plasma sheet accounts for the near constancy in the temperatures associated with increases in the ion density with Kp.

5. CONCLUSIONS

A number of important conclusions can be drawn from this preliminary statistical study. A brief summary will be given below. This report will conclude with recommendations for needed improvements in this critical analysis.

(1) Pronounced local time variations are observed in the electron moments which peak between 0000 and 0600 LT,

(2) All moments increase with Kp. This appears to be primarily the result of an increase in density since the temperature hardly varies with Kp,

(3) The electrons do not, on the average, vary significantly with L-shell while the ions increase dramatically with decreasing L-shell,

(4) The intercomparisons of parameters demonstrate similar variations to those observed by ATS-5 and ATS-6. They reveal pronounced adiabatic-like power law relationships between parameters.

Recommendations for the final atlas include:

(1) More data in order to have a more uniform statistical spread in local times, Kp, and L-shell,

(2) Analysis of the 0-100 eV SC9 data,

(3) Angular variations and ion composition statistics,

(4) Inclusion of magnetic and electric fields.

In conclusion, this analysis has been particularly useful in establishing the baseline variations in the SCATHA SC5 and SC9 particle data. Although various differences were observed, there was generally good agreement between the results from the two instruments. The results when compared with the ATS-5/ATS-6 results were also found to be in good agreement. This permitted the interpretation of the ATS-5/ATS-6 results to be applied to the SCATHA study.

References

1. Durrett, J.C., and Stevens, J.R. (1979) Description of the space test program P78-2 spacecraft and payloads, in Spacecraft Charging Technology – 1978, edited by R.C. Finke, and C.P. Pike, NASA CP-2071/AFGL-TR-79-0082, 4-10.

2. Stevens, J.R., and Vampola, A.L. (Editors) (1978) Description of the Space Test Program P78-2 Spacecraft and Payloads, SAMSO-TR-78-24.

3. Garrett, H.B., and DeForest, S.E. (1979) Time-varying photoelectron flux effects on spacecraft potential at geosynchronous orbit, J. Geophys. Res. 84:2083-2088.

4. Garrett, H.B. (1979) Review of quantitative models of the 0-100 KeV near-earth plasma, Rev. Geophys. Space Phys. 17:397-417.

5. Garrett, H.B., Schwank, D.C., and DeForest, S.E. (1980a) A statistical analysis of the low energy geosynchronous plasma environment, Part I – Electrons, submitted to Planet. Space Sci.

6. Garrett, H.B., Schwank, D.C., and DeForest, S.E. (1980b) A statistical analysis of the low energy geosynchronous plasma environment, Part II – Ions, submitted to Planet. Space Sci.

7. Hanser, F.A., Hardy, D.A., and Sellers, B. (1979) Calibration of the Rapid Scan Particle Detector Mounted in the SCATHA Satellite, AFGL-TR-79-0167.

8. DeForest, S.E., and McIlwain, C.E. (1971) Plasma clouds in the magnetosphere, J. Geophys. Res. 76:3587-3611.

9. Mauk, B.H., and McIlwain, C.E. (1975) ATS-6 Auroral particle experiment, IEEE Trans. Aerospace and Electronics System, AEA-11(No. 6):1125-1130.

10. Frank, L.A. (1971) Relationship of the plasma sheet, ring current, trapping boundary, and plasma pause near the magnetic equator and local midnight, J. Geophys. Res. 76:2265-2275.

Appendix A

Energy Band Limitations, SC5/SC9
Energy Flux Determinations

A1. INTRODUCTION

This appendix consists of three sections. The first section discusses limitations in the SC9 energy band-pass and the technique used to extend the effective range of the data. The second and third sections discuss the conversions used to obtain differential energy flux from counts for the SC5 and SC9 instruments. A complete error analysis would include a discussion of noise levels, ion composition effects, and angular anisotropies. These effects must be left to a subsequent study.

A2. ENERGY BAND-PASS LIMITATIONS

The SC9 data analysis is limited in terms of the four moments by the energy band-pass of the detectors. To estimate this effect, a Maxwellian distribution with a density of 1 cm^{-3} and a temperature range of 1 eV to 100 eV was convolved with the instrument response functions and the results integrated to give an estimate of the four moments. The ratios of the instrument-determined values to the estimated values are plotted in Figure A1 for SC9. The temperature range for which the TAVG estimates are accurate to ± 20 percent is ~ 200 eV to 24.7 keV. The TRMS estimates are accurate to ± 20 percent between ~ 100 eV and 20.6 keV. These ranges severely limit the four moment representation as the high energy component (TRMS or T2) is

often outside the 20 percent range. In order to estimate the effects this has on the results, a simple extension technique has been developed and will be described below.

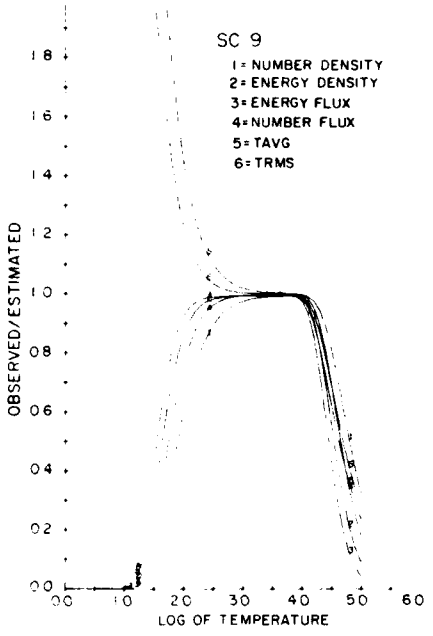

Figure A1. SC9 Instrument Response Curves for a Single Maxwellian Spectrum. Ratios of observed to estimated values are plotted vs the log of the temperature in eV

If it is assumed that the plasma is Maxwellian at high energies, a simple method for extending the effective temperature range from ~ 20 keV to 100 keV is possible. In the first step the estimated moments are converted to the 2 Maxwellian components N1, N2, T1, and T2. Next, it is assumed that the T2 instrument response is given by the ratio of [TRMS(Observed)/TRMS(Estimated)] and that T2(Estimated) is equal to T, the abscissa, in Figure A1. As the ratio [T2(Observed)/T2(Estimated)] is thus known as a function of T, it is straightforward to extend the effective range of T2 and obtain a T2(Calculated) for a given T2(Observed).

By way of illustration, we approximated the ratio ×T2(Observed)/T2(Estimated)] by:

$$\frac{Y}{X} = a_0 + a_1 (\mathrm{Log}_{10}X) + a_2 (\mathrm{Log}_{10}X)^2 + a_3 (\mathrm{Log}_{10}X)^3 + a_4 (\mathrm{Log}_{10}X)^4 + a_5 (\mathrm{Log}_{10}X)^5 \quad \text{(A1)}$$

where

Y = T2(Observed)

X = T2(Estimated)

a_0, -----, a_5 = constants determined by a least squares fit to Figure A1.

If T2(Observed) is 15 keV, then the solution of Eq. (A1) by iteration gives a T2(Calculated) of 17 keV for SC9.

The same procedure can be employed for N2. If N2 is assumed equivalent to ND so that the ratio [N2(Observed)/N2(Estimated)] that is, [ND(Observed)/ND(Estimated)] is as determined in Figure A1, then N2(Calculated) can be obtained from:

$$N2\ (\text{Calculated}) = [N2(\text{Observed})/N2(\text{Estimated})]^{-1} \cdot N2(\text{Observed}) \qquad (A2)$$

where the ratio in brackets is given by:

$$\frac{W}{X} = b_o + b_1 (\text{Log}_{10}X) + b_2 (\text{Log}_{10}X)^2 + b_3 (\text{Log}_{10}X)^3 + b_4 (\text{Log}_{10}X)^4 + b_5 (\text{Log}_{10}X)^5 \qquad (A3)$$

where

W = N2(Observed

X = N2(Estimated)

b_0, -----, b_5 = constants determined by a least squares fit. If N2(Observed) is 1 cm^{-3} and T2(Observed) is 15 keV, this procedure gives an N2(Calculated) of 1.03 cm^{-3} for SC9.

It is next assumed that N1 and T1 are not affected by the energy bandpass. Given N1, T1, N2(Calculated) and T2(Calculated), the new moments are calculated. In tests the method yielded results to an accuracy of 5 percent or better up to 100 keV.

All the statistical variations for SC9 were determined using the above calculated values. The largest changes were in T2 and energy flux for the ions. The electron averages changed by less than 10 percent. There was little change in the qualitative shapes of the curves or their relationship to each other by using the calculated values rather than the original observed values. Statistically the only differences introduced by the band-pass limitations are in the absolute scale values.

A3. SC5 DIFFERENTIAL ENERGY FLUX DETERMINATION

For SC5 the average counts in each energy channel for 10-min intervals were calculated. Since the SC5 detector samples all channels once per second, this corresponds to 600 measurements for each average value. The average counts were converted into count rates by dividing by 0.2-sec accumulation interval for each sample. The count rates were then converted to differential energy flux according to the equation:

$$\frac{d(EF_i)}{dE} = \frac{\bar{E}_i C_i}{G_i \Delta E_i} \tag{A4}$$

where

C_i = average counts per second in energy channel i,

$\bar{E}_i$ = average energy of particles in that channel,

G_i = the peak geometric factor in channel i,

ΔE_i = the width in energy of channel i.

(The values used for E_i, G_i, and ΔE_i are listed in Tables 3, 5, 8 and 10 of Hanser et al.)[7]

A4. SC9 DIFFERENTIAL ENERGY FLUX DETERMINATION

For SC9 an average counts per energy channel was created. The counts were first converted to count rates by division by 0.25 sec, the sampling interval. The count rates were then converted to differential energy flux according to the following:

$$\frac{d(EF)_i}{dE} = \frac{C_i}{H \cdot e_i} \tag{A5}$$

where

C_i = average counts per sec per energy channel,

e_i = energy in eV,

H = 1.6×10^{-4} cm^{-2} - sr^{-1}, for electrons,

= 3.3×10^{-4} cm^{-2} - sr^{-1}, for ions,

e_i = $e_1 \cdot e_2$ for electrons,

= e_3 for ions,

e_1 = $1 - 2/(3 + 6.5/(E(keV) + 0.2) + 30./(E(keV) + 0.2)^3)$

e_2 = $1 + 2/((E(keV)/0.15)^3 + 1)$,

e_3 = $1 + 2/((E(keV)/1.5)^3 + 1)$.

The energy steps are given by:

$$E = -21 + 16.1x\,(1.45^S) + 28/(M+1) \qquad \text{(A6)}$$

where

$M = 12 + S$

S = step (0 to 63).

There is a temperature correction but it is small above 100 eV. Also a sun pulse was occasionally observed and it was not deleted in the north-south data used in this study.


DAT
FILM